

Refill of Droplet-On-Demand Inkjet Actuators

S.G. Mallinson^{1,2,*}, G.D. McBain¹, G.D. Horrocks¹, B.R. Brown¹ and P.J. Reichl¹

¹ Memjet, Macquarie Park NSW 2113, Australia

² University of New South Wales, Kensington NSW 2052, Australia

*Email: sam.mallinson@memjet.com

Abstract

After a droplet-on-demand inkjet actuator fires a droplet, the ink chamber must be replenished before a subsequent firing. Otherwise, the resulting droplet volume can be smaller than desired, and, the droplet tail can extend further and break into a larger number of small satellites that can contribute to image quality issues and waste aerosol. The refill flow into the chambers is driven by the difference between the capillary pressure of the ink meniscus in the chamber and nozzle, and the ink supply pressure. Here, we describe modelling of the refill flow, including the hydrodynamics of refill and the capillary pressure of the ink meniscus; we also compare models with experimental data.

1 Introduction

Inkjet printing involves firing a sequence of droplets at a surface to create text and images for documents, labels and packaging. Inkjet technology is also used in non-traditional printing processes, for example additive manufacturing, printed electronics and pharmaceutical labelling. After each droplet is fired, ink must refill the firing chamber before subsequent ejections. Otherwise, the droplets produced can have a different diameter and so cause a variable printed image density. An under-filled chamber can also cause the ejected liquid meniscus to form a long slug of ink that can break into several smaller droplets. These smaller droplets can result in undesirable image density variations, and also cause internal and external surface fouling and consequent unacceptable media marking. The smaller droplets can also exit the printing system, resulting in operator health and safety issues. Thus, refill of inkjet firing chambers is a key issue in the design of inkjet printers.

A schematic of a thermal inkjet firing chamber is shown in Figure 1. Ink enters the chamber via a feedhole connected to the supply by a dendritic network of ducts; only the channel, formed by etching of the back side of the chips, is shown in the schematic. The chamber is capped with a nozzle, through which ink is forced to form droplets. Refill of the firing chambers occurs due to the capillary suction of the meniscus which is situated in the nozzle and chamber.

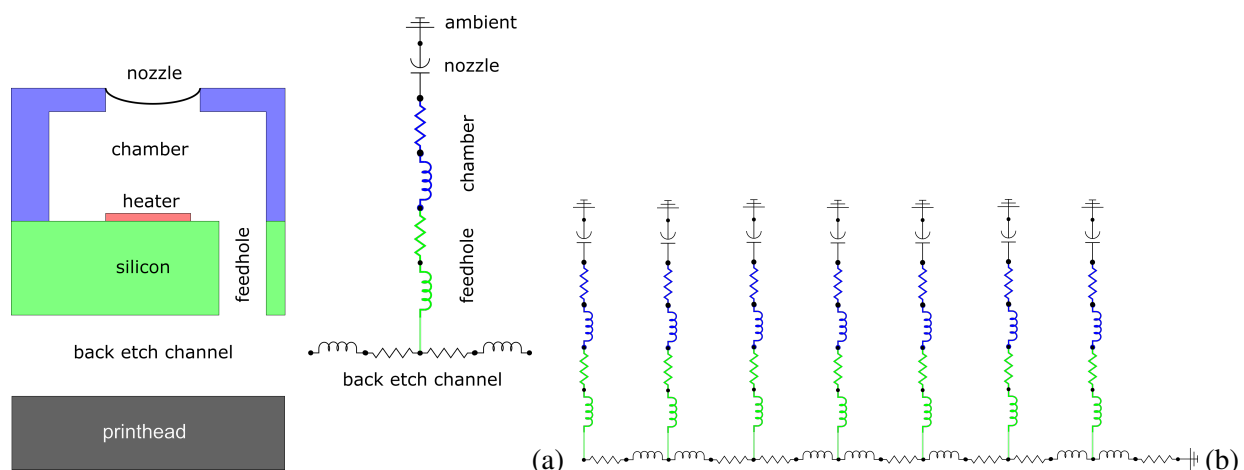


Figure 1. (a) Schematic of inkjet firing chamber, with equivalent fluid circuit; (b) Simple network consisting of seven actuators connected to a short section of back etch channel.

The refill process can be modelled using computational fluid dynamics although this become unwieldy for large networks. For example, for Memjet printheads, there are more than seventy thousand nozzles in a



printhead, so if one million mesh elements are required for a model of a single actuator, which is typical, more than seventy billion elements would be required to simulate flow in the entire printhead. Further, the simulation of capillary flows can be inaccurate for volume-of-fluid models, due to the moving contact line paradox (Shikhmurzaev, 2001). Thus, it is more convenient to use lumped element models based on the electrical analogy, with electrical resistance, inductance and capacitance being equivalent to fluid resistance, R , inertance, L and compliance, C , respectively (Kirshner & Katz, 1975). Methods for computing these parameters are discussed later in this paper. For single lump problems, the flow over time t can be modelled using the one-dimensional hydraulic equation in terms of flow rate Q and pressure p , with (Kirshner & Katz, 1975):

$$L \frac{\partial Q}{\partial t} + RQ + \int \frac{Q}{C} dt = \Delta p \quad (1)$$

For more complex problems, a network approach is used.

Here, we discuss solutions to eq. (1) under a number of simplifying assumptions and demonstrate the use of such solutions for engineering purposes. Further, we discuss how flow in a network of components can be simulated and present examples from practical industrial systems.

2 Computing resistance, inertance and compliance

2.1 Resistance

Hydraulic resistance is the ratio of the driving pressure difference to the volumetric flowrate it produces at steady state (Kirshner & Katz, 1975). For the relatively simple case of flow in long straight ducts, under laminar conditions consistent with the low Reynolds number of the flow, the problem of computing hydraulic resistance reduces to the solution of a plane Poisson equation, though “fully developed flow is seldom reached in fluidic passages” (Kirshner & Katz, 1975). For a long straight duct of length ℓ and constant cross-sectional area A , the hydraulic resistance is given by $R = \mu\ell/(kA^2)$, where k is the Boussinesq k -factor (Dryden *et al.*, 1956). For practical geometries, one needs to solve the steady Stokes or Navier-Stokes equations and evaluate the flow rate through a port due to the pressure difference between ports.

2.2 Inertance

Hydraulic inertance is the property of a fluid flow branch that opposes changes in flow rate. Consider the flow rate shortly after a step-change in pressure difference: $\Delta p = P_-$ for $t < 0$ and $\Delta p = P_+$ for $t > 0$. If the hydraulic compliance is nonzero, the only volume history compatible with the pressure difference for the infinite time up to time zero is $V = CP_-$. Thus the initial conditions before the step in the pressure difference, that is, at $t = 0_-$ are $V = \int Q dt = CP_-$ and $dV/dt = 0$. For early times after the step, the Maclaurin series in time for the volume is:

$$V(t) \sim V(0) + t\dot{V}(0) + \frac{t^2}{2}\ddot{V}(0) + O(t^3) \sim CP_- + \frac{t^2}{2}\ddot{V}(0) + O(t^3) \quad (2)$$

So, for early times, the lumped-parameter hydraulic equation reduces to $L = (P_+ - P_-)/\ddot{V}(0)$. Thus, the inertance can be computed as the ratio of the suddenly applied change in pressure difference to the rate of change of flow rate. The corresponding jump in the flow rate can be used to define the inertance (Asai, 1991; Deshpande, 1996; Cornell, 1998). For the case of uniform density, the inertance is computed from either the inlet or outlet formula below:

$$L \equiv \frac{I}{\iint_{\text{inlets}} \mathbf{n} \cdot \nabla \left(\frac{\Pi}{\rho} \right) dA} = \frac{I}{-\iint_{\text{outlets}} \mathbf{n} \cdot \nabla \left(\frac{\Pi}{\rho} \right) dA} \quad (3)$$

where Π is the solution of:

$$\begin{aligned} \nabla \cdot \left(\frac{1}{\rho} \nabla \Pi \right) &= 0 && \text{throughout flow domain} \\ \Pi &= \begin{cases} I, & \text{on inlets} \\ 0, & \text{on outlets} \end{cases} && (4) \\ \frac{1}{\rho} \frac{\partial \Pi}{\partial n} &= 0 && \text{on walls.} \end{aligned}$$

where ρ is density. For a long straight duct of constant cross-sectional area, the hydraulic inertance is given by $L = \rho \ell / A$.

2.3 Compliance

An element of a hydraulic network is compliant if its volume increases with the pressure across it; following Kirshner & Katz (1975), we define compliance as the ratio of the storage of volume flow to the change in pressure. Hydraulic compliance can result from several mechanisms, such as: a pinned meniscus; suspended bubbles; distensibility of the solid walls; and, compressibility of the fluid.

In inkjet actuators, the nozzle plays an important role in providing a suction pressure to induce refill flow into the firing chamber. In the first instance, we attempted to find analytical solutions to this problem: we assumed the contact line (where the meniscus meets the wall) is a plane closed loop (the entrance to the nozzle). Depending on the contact angle and the geometry, this should be the case for a range of liquid volumes. If gravitational forces are negligible, the surface should have constant mean curvature, $K_m \equiv \kappa_1 + \kappa_2 \equiv 1/r_1 + 1/r_2$, since that is related to the pressure by the Young–Laplace equation, $p = \sigma K_m$, where σ is the surface tension. Gravitational forces are negligible if the Bond number $Bo \equiv \rho g h^2 / \sigma$ is small; that is, if the height h is small compared to the characteristic capillary length $(\sigma / \rho g)^{1/2}$. Here, values of h are of the order of microns and capillary lengths are of the order of millimetres, so a zero Bond number model is appropriate.

2.3.1 Circular nozzle

The meniscus pinned at a circle, which is a commonly encountered nozzle shape, is an important special case of the problem of the suction of pinned menisci since it has a simple exact solution (at zero Bond number): the meniscus is a spherical cap. The surfaces of uniform mean curvature bounded by a circle of radius R_n (and so area $A_n = \pi R_n^2$) are spherical caps of (spherical) radius R and height h such that $R = (R_n^2 + h^2) / 2h$. The volume is $V = \pi h(3R_n^2 + h^2) / 6 = \pi h(3A_n / \pi + h^2) / 6$ and the pressure is $p = 2\sigma / R = 4\sigma h / (R_n^2 + h^2) = 4\sigma h / (A_n / \pi + h^2)$. Notice that the pressure goes through a maximum value $2\sigma / R_n$ when $h = R = R_n$ and $V = 2\pi R_n^3 / 3$ (López & Montiel, 1996) - this is the hemisphere on the bounding circular loop. Thus the pressure–volume relation is invertible only for $0 < h < R_n$. If the meniscus is pressure-controlled (rather than volume-controlled as in the procedure described above), the meniscus becomes unstable when the pressure exceeds this maximum (Michael, 1981).

We can write the following expression for the ullage of the meniscus, normalized by the volume of a hemisphere with radius R_n , denoted \bar{V} , in terms of the pressure normalized by the capillary pressure for R_n , $\bar{p} = p / (2\sigma) \sqrt{A_n / \pi} = R_n / R$:

$$\bar{V} = \frac{1}{\bar{p}^3} \pm \left(\frac{\sqrt{1 - \bar{p}^2}}{\bar{p}^3} + \frac{\sqrt{1 - \bar{p}^2}}{2\bar{p}} \right) \quad (5)$$

where the positive and negative values are for $\bar{V} \leq 1$ (ullage less than hemispherical cap) and $\bar{V} \geq 1$ (ullage greater than hemispherical cap), respectively. The compliance is obtained as the gradient of volume with respect to pressure:

$$C = \frac{dV}{dp} = \frac{\pi R_n^4}{3\sigma} \frac{d\bar{V}}{d\bar{p}} \quad (6)$$

and so after some simplification:

$$\bar{C} = \frac{C}{C_r} = \frac{-2\sqrt{1 - \bar{p}^2} \pm (\bar{p}^2 - 2)}{\bar{p}^4 \sqrt{1 - \bar{p}^2}} \quad (7)$$

where $C_r = \pi R_n^4 / (2\sigma)$. The variation of the \bar{p} and \bar{C} as a function of \bar{V} are shown in Fig. 2(a).

2.3.2 Elliptical nozzle

For arbitrary shapes, the asymptotic expansion for pinned menisci at low curvature is of the form:

$$h \sim \sum_{i=1}^{\infty} \left(K_m \sqrt{A} \right)^{2i-1} h_{2i-1} \quad (K_m \sqrt{A} \rightarrow 0). \quad (8)$$

For an ellipse, when the capillary pressure is small, the deflection h of a meniscus pinned at an ellipse with semi-axis a and b satisfies the same plane Poisson equation with the same homogeneous Dirichlet boundary conditions as the longitudinal velocity in the problem of the hydraulic resistance in long straight ducts of

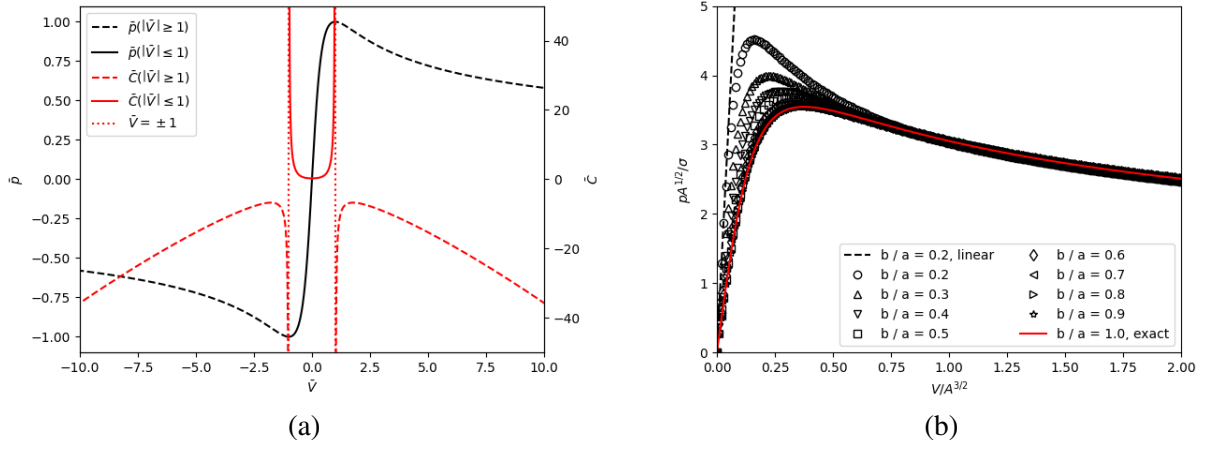


Figure 2. (a) Meniscus pressure and compliance as functions of meniscus ullage for a circular nozzle; (b) Comparison of numerically determined suction pressure as a function of volume for ellipses with varying aspect ratio, analytical value for aspect ratio unity (circle) and linear value for $b/a = 0.2$.

elliptic section. Here the forcing constant K should be interpreted as K_m , the mean curvature, which is equal to the ratio of the capillary pressure to the surface tension by the Young–Laplace law; thus:

$$\frac{h}{\sqrt{A}} \sim 2k \left(K_m \sqrt{A} \right) \left\{ 1 - \left(\frac{x}{a} \right)^2 - \left(\frac{y}{b} \right)^2 \right\}, \quad (K_m \sqrt{A} \rightarrow 0) \quad (9)$$

where $A = \pi ab$ and $k \equiv \frac{a/b}{4\pi\{1+(a/b)^2\}}$. The volume between the meniscus and its original plane has a corresponding asymptotic expansion:

$$V \sim A^{3/2} \sum_{i=1}^{\infty} k_{2i-1} \left(K_m \sqrt{A} \right)^{2i-1} \quad (K_m \sqrt{A} \rightarrow 0) \quad (10)$$

$$\text{where } k_j \equiv A^{-3/2} \int_{\Omega} h_j d\Omega. \quad (11)$$

This closed-form solution can be used to deduce asymptotes for some quantities of interest, such as the volume $V \equiv \int z dA$ which is directly related to the Boussinesq k-factor for ellipses:

$$\frac{V}{A^{3/2}} \sim k \left(K_m \sqrt{A} \right) \quad (K_m \sqrt{A} \rightarrow 0) \quad (12)$$

2.3.3 Arbitrary nozzle shape

For a general nozzle shape, we resort to numerical methods: either using a minimum surface energy calculation as embodied in the Surface Evolver tool (Berthier & Brakke, 2012) or a membrane deflection calculation which we have implemented in both finite volume - OpenFOAM (Greenshields & Weller, 2022) - and finite element - FreeFEM++ (Hecht, 2012) and scikit-fem (Gustafsson & McBain, 2020) - solvers. Figure 2(b) compares the results from Surface Evolver for ellipses of varying aspect ratio with the analytical expression for a circle and the small curvature asymptote for $b/a = 0.2$.

3 Solutions to the one-dimensional hydraulic equation

3.1 Simple models of refill without inertance

Refill is driven by the difference between the supply pressure p_s and the pressure on the liquid side of the meniscus, p . In the absence of inertance, the volume of liquid evolves with time t according to:

$$R dV = (p_s - p) dt, \quad (13)$$

This equation is trivially true in that it follows immediately from the definition of hydraulic resistance as the ratio of pressure difference to volumetric flow rate; it becomes a model by positing relations between R , V , p ,

and t , for example that the hydraulic resistance is constant and that the meniscus suction $-p$ is some function of the ullage $-V$.

There are a number of reasons to investigate solutions where inertance is neglected. First, for small values of inertance, the timescale equal to the ratio of inertance to resistance, $\tau = L/R$, can be much shorter than the known timescale of refill. Typical values of R and L for inkjet designs produced by Memjet are of order $R = 10^{14}$ Pa s/m⁻³ and $L = 10^8$ kg/m⁻⁴, so the inertance/resistance timescale is about a microsecond. This is two orders of magnitude less than the refill timescale of a hundred microseconds corresponding to the reciprocal of an actuation frequency of 10 kHz. Thus a priori we expect inertance to have a negligible effect on refill for a range of inkjet designs produced by Memjet. Second, the underlying hydraulic equation is a first-order ordinary differential equation and there are many special techniques for such problems (Ince, 1956) that are not applicable to second-order systems such as those with inertance. Thus we are motivated to persist with the fiction of zero inertance in order to obtain closed-form solutions. Third, by observing the differences between models without inertance and real systems we might better understand those phenomena which are due to factors other than inertance and so by elimination understand which effects are peculiar to inertance.

We consider an arbitrary initial condition $V = V(0)$ at $t = 0$. Typically this is negative, depending on where we take the datum for volume, a drop having just been ejected. From the solution $V(t)$ of the initial value problem we can compute the zero-frequency drop volume from $V_d = V(\infty) - V(0)$, assuming $\lim_{t \rightarrow \infty} V(t)$ exists, is finite and greater than $V(0)$. For well-designed systems we expect $V(\infty)$ to be independent of $V(0)$ at least if $V(0)$ is in some range; we expect the asymptotic volume to represent a stable equilibrium with a finite basin of attraction. Of course $V(\infty)$ will depend on p_s .

Ejecting again before $V(t)$ has converged to $V(\infty)$ should result in a reduction in drop-volume. A simple model for this is that the shortfall in drop-volume is equal to the shortfall of refill; equivalently, the volume $V(0)$ after ejection is constant, independent of drop volume.

Refill seems to be reasonably well characterized by a constant hydraulic resistance. A constant resistance corresponds to the dominance of an upstream obstruction such as a baffle. It differs from the capillary filling of a long thin pipe as considered by Washburn (1921) for which the resistance is proportional to the wetted length of pipe and therefore R is proportional to V . If both hydraulic resistance and meniscus suction pressure $p = -s$ are constant the equation can be integrated directly to give $V(t) = V(0) + (p_s + s)t/R$. We get zero volume for $t = -RV(0)/(p_s + s)$, which can therefore be construed as the ‘refill time’. Subsequently the volume continues to increase without bound; this is unphysical.

A constant pressure difference corresponds to a meniscus moving without deformation along a capillary pipe of constant section, as in the study of Washburn. In an inkjet printer this would mean a nozzle much longer than those used in typical devices.

The unphysical continued unbounded increase of volume can be removed by switching the meniscus suction to balance the supply suction $-p_s$ at some volume $V(\infty) > V(0)$:

$$P(V) = \begin{cases} -s, & V < V_\infty; \\ p_s, & V \geq V_\infty \end{cases}$$

The volume history is correspondingly modified to:

$$V(t) = \begin{cases} V(0) + \frac{(p_s + s)t}{R}, & t < t_H; \\ V_\infty, & t_H < t, \end{cases}$$

(14)

where $t_H \equiv \frac{\{V_\infty - V(0)\}R}{p_s + s}$

The volume now never reaches zero, assuming $V(\infty) < 0$, corresponding to $p_s < 0$, but there is still an obvious refill time-scale: $V(\infty) - V(0)R/(p_s + s)$.

In general the meniscus pressure p will depend on the volume V . In this case, provided the resistance and supply pressure are constant and the meniscus suction depends on time not explicitly but only via a dependence on volume, then in eqn.(14), the variables separate and each side can be integrated directly (Ince, 1956):

$$\frac{t}{R} = \int_{V(0)}^{V(t)} \frac{dV}{p_s - p(V)}. \quad (15)$$

Actually the meniscus suction will depend on time because the dynamic surface tension of the ink will decrease as surfactants migrate to the surface, but we neglect that in the simple models analysed here.

If the meniscus is pinned at the entrance to the nozzle, the capillary suction it exerts on the liquid decreases as it pulls in more liquid. For small displacements (ullages) it is reasonable to linearize this and say $p = V/C$,

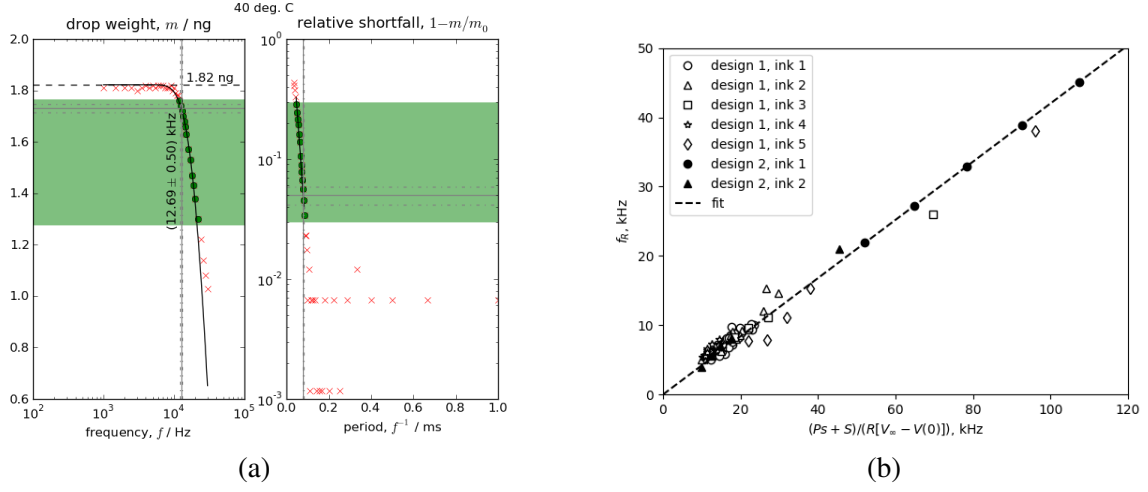


Figure 3. Experimental droplet weight data. (a) Curve fitting of droplet weight-frequency sweep. $m_d(0) = 1.82$ ng, $f_s = 12.7$ kHz and $RC = 17.8$ μ s; (b) Correlation of refill frequency as a function of the ratio of suction pressure to the product of droplet weight.

where the constant C is the hydraulic compliance of the system, which is something like the reciprocal of the stiffness of the meniscus considered as a spring. The flow equation can be integrated to give:

$$V = V_\infty - \{V_\infty - V(0)\}e^{-t/RC}, \quad (16)$$

where $V_\infty \equiv Cp_s$. The volume decreases exponentially to an eventual value $V_\infty = Cp_s$ with a time constant RC . This asymptotic volume will have the same sign as the supply pressure; typically both are negative. The capacitance should be positive or the system will be mechanically unstable, either depriming ($V \rightarrow -\infty$) or flooding ($V \rightarrow +\infty$) depending on the initial conditions. In the case of constant pressure, the refill time is proportional to the drop volume, whereas in this case of constant compliance, the exponential time constant is independent of the drop volume and depends only on the viscous resistance of the system and the compliance of the meniscus.

Eventually as $t \rightarrow \infty$, the system should approach refill; i.e. $V \rightarrow V(\infty)$, with $p(V_\infty) = p_s$. Toward this time, if the system is almost refilled, $V \rightarrow V_\infty$, we can expand the pressure–volume relation in a Taylor series:

$$p(V) \sim p(V_\infty) + (V - V_\infty)p'(V_\infty) = p_s - \frac{V_\infty - V}{C}, \quad (17)$$

where $C \equiv 1/p'(V_\infty)$ is the marginal compliance at equilibrium.

According to this, the ullage should ultimately decay exponentially. Integrating from some time t_1 after which the volume is close enough to its equilibrium value that truncation of the Taylor series as above is acceptable:

$$\frac{V_\infty - V(t)}{V_\infty - V(t_1)} \sim e^{-(t_1 - t)/RC}. \quad (18)$$

The above Heaviside and linear models are still unphysical (except for the asymptotically linear model, but that is not complete). The suction should be a continuous bounded function of ullage, whereas the Heaviside model requires a jump in the suction to prevent unbounded volume and the linear law admits arbitrarily large suctions for large ullages. These two defects can be overcome by combining the two laws piece-wise:

$$V(t) = \begin{cases} V(0) + \{V_\infty - V(0)\}t/t_H, & 0 < t < t_H - RC; \\ V_\infty - \{V_\infty - V(0)\} \frac{RC}{t_H} \exp\left(\frac{t_H - t}{RC} - 1\right), & t_H - RC < t. \end{cases} \quad (19)$$

3.1.1 Drop-weight frequency-sweeps for simple models of refill without inertance

The long-time asymptotic analysis of the simple models of refill without inertance showed that the volume should eventually refill like eqn.(14). Here we consider the analysis of low-frequency drop-weight data in terms of this model as a means of rationally extracting ‘refill times’ from experimental drop-weight frequency-sweeps using a single-chip test printhead, with the dendritic component replaced by a large reservoir with very

small inertance. In these experiments, several thousand droplets are ejected from the chip into a beaker placed on an accurate balance, and, with accounting for evaporative losses, the average mass is calculated. The test is repeated at a number of different frequency values. Based on eq.(19), we propose fitting the data to the form:

$$\ln \left\{ 1 - \frac{m_d(f)}{m_d(0)} \right\} = \frac{t_0 - 1/f}{RC}, \quad (20)$$

where $m_d(0) = \rho V(0)$ is the zero-frequency drop-weight and t_0 and RC are two fitting parameters (dimensionally both time constants).

The parameter t_0 in the fit has no direct physical significance, unlike RC , which is the asymptotic timescale of the decay of the ullage. Instead it can be replaced with a parameter that does, such as the frequency f_s corresponding to a given relative shortfall S , so $\ln S \equiv (t_0 - 1/f_s)/RC$ and:

$$\ln \frac{1 - m_d(f)/m_d(0)}{S} = \frac{f_s^{-1} - f^{-1}}{RC}. \quad (21)$$

We suggest, say, $S = 0.05$, which might correspond to a shortfall near the limits of perception in terms of print quality and also be simultaneously beyond the noise in good experimental data and within the range for which the linearization implied in the above fit is reasonable.

If $m_d(0)$ can be determined by inspection, these constants can be determined by linear regression: plot $y \equiv \ln \{1 - m_d(f)/m_d(0)\}$ as a function of $x \equiv 1/f$ and find the line of best fit $p_0x + p_1$ to y , then $RC = -1/p_0$ and $f_s = \frac{p_0}{\ln S - p_1}$. The predicted drop-weight from the fit is $m_d(f) = m_d(0) \left\{ 1 - S \exp \frac{f_s^{-1} - f^{-1}}{RC} \right\}$. An example is shown in Fig. 3(a), with the fitting constants: $m_d(0) \approx 1.82$ ng, $f_s \approx 12.7$ kHz and $RC = 17.8$ μ s.

3.2 Comparison of refill frequency for different actuator designs and inks

The refill frequency data has been measured for many different actuator designs - for example, with different nozzle, chamber and feedhole dimensions - and a number of inks with a range of viscosity and surface tension values. Considering the simple case of constant suction pressure, eqn.(14), we can write a proposed scaling for the refill frequency as:

$$f_R \approx \frac{\Delta p}{RV_d} \quad (22)$$

where $\Delta p = p_s - s$. The data are compared in Fig. 3(b), and it can be seen that the data follow a linear fit. This allows estimation of refill frequency for new designs prior to their manufacture.

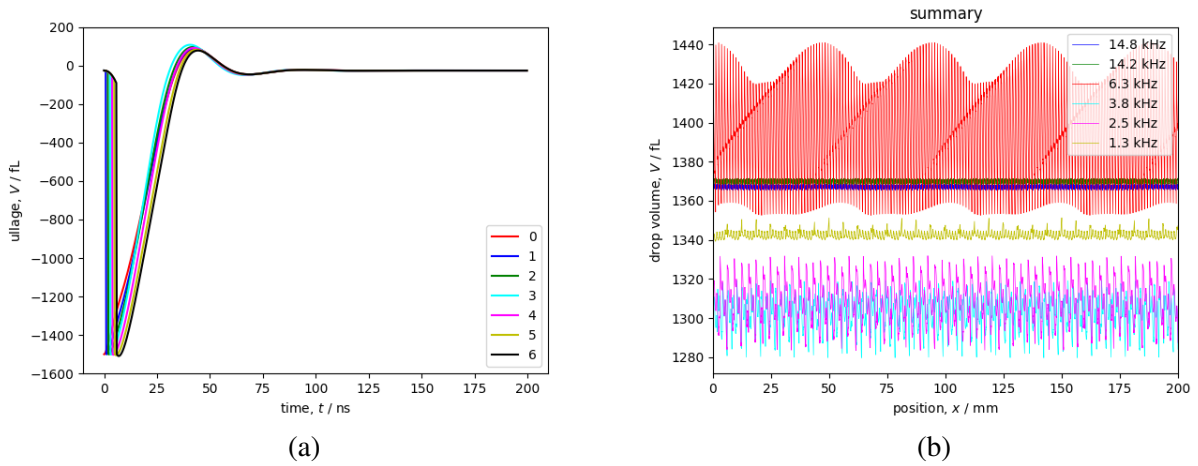


Figure 4. (a) Refill response of circuit shown in Figure 1(b); (b) Response of single colour plane (14080 actuators) as a function of firing frequency.

4 Network modelling

For a typical printing system, there will be numerous inkjet actuators which produce droplets and then refill. If the printing system extends into the larger parts of the printhead, then the small inertance assumptions used

above are no longer valid. Thus, to obtain information about refill, we have simulated the system by constructing network or circuit models, which are then analysed using a circuit simulator. Some initial calculations were performed using freely available SPICE circuit simulators (Nagel & Pederson, 1973). These proved to be limiting, for example, it was possible but not straightforward to implement non-linear compliance models due to meniscus motion during refill. So we developed an in-house, Python-based solver called ‘Millihydraulics’, and two examples of its use are presented below.

In the first example, the circuit consists of a small network of actuators connected together along a common rail representing the channels in the back of the chip, see Figure 4(a). The results, shown in Figure 4(b) show the refill after the nozzles are fired one after the other, with one microsecond delay between each of the seven consecutive ejections. For this case, the refill overshoots before the oscillations decay, indicative of a slightly underdamped system.

A second example is a single colour plane consisting of 14080 nozzles arranged along a printhead of approximately 200 mm in length. Figure 4(c) shows the simulated response of the network for a range of different firing frequencies, corresponding to different paper printing speeds. The variation of droplet volume along the printhead is less than one percent of the average volume for the lowest and two highest frequencies, but is approximately seven percent at 6.3 kHz. This would result in clearly visible optical density banding on the printed image at a pitch of approximately 47 mm. At 2.5 kHz and 3.8 kHz, although the volume variation is about half that predicted for 6.3 kHz, the pitch is much finer, which would be less objectionable on the final print.

5 Conclusions

Refill of inkjet firing chambers has been analysed using the lumped hydraulic equation. The nozzle capillary suction has been described in terms of the meniscus ullage with a closed form presented for circular and elliptical nozzle shapes. A number of simple models of refill which neglect fluid inertance have been presented, and these are used to analyse experimental droplet weight - frequency sweeps, and to correlate refill frequency as a function of chamber geometry and ink rheology. Finally, a fluid circuit simulator has been used to simulate refill of inkjet printing systems.

References

- Asai, A. 1991, Bubble Dynamics in Boiling Under High Heat Flux Pulse Heating, *ASME J. Heat Transf.*, **113**, 973–979.
- Berthier, J. and Brakke, K.A. 2012, *The Physics of Microdroplets*, Scrivener.
- Cornell, R. 1998, Nucleation Quality and Bubble Momentum and Their Effect on Droplet Velocity and Stability, in Proc. IS&T Int. Conf. on Digital Printing Tech. (NIP14), 9–14.
- Deshpande, N.V. 1996, Significance of Inertia and Resistance in Fluidics of Thermal Ink-Jet Transducers, *J. Imaging Sci. & Tech.*, **40**, 396–400.
- Dryden, H.L., Murnaghan, F.P. and Bateman, H. 1956, *Hydrodynamics*, Dover.
- Greenshields, C. and Weller, H. 2022, *Notes on Computational Fluid Dynamics: General Principles*, CFD Direct Ltd.
- Gustafsson, T. and McBain, G.D. 2020, ‘scikit-fem’: A Python Package for Finite Element Assembly. *J. Open Source Software*, **5**, 2369.
- Hecht, F. 2012, New Development in FreeFem++, *J. Num. Math.*, **20**, 251–266.
- Ince, E.L. 1956, *Ordinary Differential Equations*, Dover.
- Kirshner, J.M. and Katz, S. 1975, *Design Theory of Fluidic Components*, Academic Press.
- López, R. and Montiel, S. 1996, Constant Mean Curvature Surfaces with Planar Boundary, *Duke Math. J.*, **85**, 583–604.
- Michael, D.H. 1981, Meniscus Stability, *Ann. Rev. Fluid Mech.*, **13**, 189–215.
- Nagel, L.W. and Pederson, D.O. 1973, SPICE (Simulation Program with Integrated Circuit Emphasis), University of California, Berkeley, Tech. Rept. No. UCB/ERL M382.
- Shikhmurzaev, Y. D. 2001, Dynamic Wetting: Issues Resolved and Raised, in IUTAM Symposium on Free Surface Flows, Volume 62 of Fluid Mechanics and its Applications, Kluwer Academic, 19–28.
- Washburn, E.W. 1921, The dynamics of capillary flow, *Phys. Rev.*, **17**, 273–283.